# Self-healing properties of flaws in nanoscale materials: Effects of soft and hard molecular dynamics simulations and boundaries studied using a continuum mechanical model

Yufeng Guo and Wanlin Guo*
*Institute of Nanoscience, Nanjing University of Aeronautics and Astronautics, Nanjing, 210016, China*
(Received 29 September 2005; published 16 February 2006)

Soft and hard boundary effects on the flaw in self-healing capabilities of the nanoscale copper clusters and biomaterials have been studied using molecular dynamics simulations as well as the theoretical analyses. When the copper nanocluster size decreases to a compatible magnitude to its flaw, different boundary conditions change the flaw self-healing capability and lead to different dislocation generation and atom rearrangement after the copper nanocluster is healed. The theoretical predictions for the copper nanocluster are in good agreement with the molecular dynamics simulations. Further theoretical investigations demonstrate that the mineral layer in biomaterials possess a high flaw self-healing capability because of the nanometer scale and natural soft boundaries caused by the stacking protein and aragonite layered structures.

DOI: 10.1103/PhysRevB.73.085411 PACS number(s): 61.46.−w, 87.68.+z, 83.60.Uv, 71.15.Pd

## I. INTRODUCTION

Since the last decade with the rapid development of nanotechnology and nanoscience, people have devoted time to fabricate and synthesize artificial nanoscale materials such as nanowires, nanotubes, nanodots, and nanoclusters.[1–4] But when size goes down to nanoscale, the surface and boundary effects become significant in these nanoscale materials. Many superior physical, electronic, and mechanical properties are discovered due to the strong size and boundary effects, which have great potential applications in many fields.[5–10] On the other hand, living organisms produce nature-evolved nanoscale materials with physical properties that still surpass those of analogous synthetic materials with similar phase compositions.[11–15] Well known examples include tooth, bone, and mollusk shells, which exhibit soft (protein) and hard (mineral) laminated structures with a thickness from a few nanometers to hundreds of nanometers.[16–26] In biomaterials, such as the abalone shell, the interactions between the mineral and protein layers produce the hard and soft boundary effects on each material, respectively, because of their great difference in elastic modulus.

Various kinds of defects such as flaw and crack have inevitably existed in those nanoscale materials and influence their properties and structures, whereas materials have the capability to repair their flaws. Presented under the proper condition, the flaw or crack will heal automatically.[27,28] But at nanoscale, the stability of a flaw may be quite different from the macroscopic scale and the strong boundary effects may change the flaws self-healing capability. Unfortunately, the boundary effects on flaws self-healing in nanoscale materials were seldom considered in the previous studies.

In our study, we chose the copper (Cu) nanocluster as an example of nanoscale material. Molecular dynamics (MD) simulations show that the free and rigid boundaries applied on the surfaces of the Cu nanoclusters yield a significantly different self-healing capability for the same defected structures. The self-healing process can be seen as the adhesion and bonding of two surfaces of the flaw. We have therefore developed the theoretical procedure presented by Yu and Suo[27] under the free, rigid displacement boundary conditions. The obtained theoretical predictions agree well with our MD results. Furthermore, the theoretical model has been used to investigate the boundary effects on the nanoscale biomaterials. It is found that the stacking protein and aragonite layered structures in biomaterials provide a high flaw self-healing capability for the mineral layers.

## II. MD SIMULATIONS

The molecular dynamics technique, which is based on Newton' law, has been employed to study the flaws of self-healing of the Cu nanocluster because it is a powerful tool and widely used in nanoscale science. In our simulations, the empirical embedded atom method (EAM) potential,[29] parametrized for the copper atom, is used to describe the interactions between Cu atoms. The time step of the MD simulations is chosen to be 1 fs and the Nose-Hoover thermostat is used to control the temperature.

First, a 7100-atom Cu nanocluster has been set up and a cleavagelike flaw is introduced by removing two rows of atoms, as shown in Fig. 1(a). The length, height, and width of the nanocluster are 9.04, 5.24, and 1.81 nm, respectively. Free and rigid boundary conditions are applied to the nanoclusters top and bottom surfaces. After a relaxation of 100 ps at 300 K, the cleavage is closed completely under both free and rigid boundaries, and one and two dislocations are generated in the clusters, respectively, which are denoted in Fig. 1(a). Then we introduce the same cleavagelike flaw and boundary conditions to a smaller 3100-atom Cu nanocluster. The width and length of this cluster are the same as that of the 7100-atom cluster, but the height deceases to 2.53 nm and the corresponding $L/h$ increases to 5.71. Under free boundaries, the flaw is healed after relaxing for 100 ps at 300 K, as shown in Fig. 1(b). But for the case of rigid boundary conditions, the same flaw still remains in the cluster after 100 ps. Different from the free boundaries, increasing the $L/h$ of the nanocluster under rigid boundaries the cleavagelike flaw becomes more difficult to be healed.

 

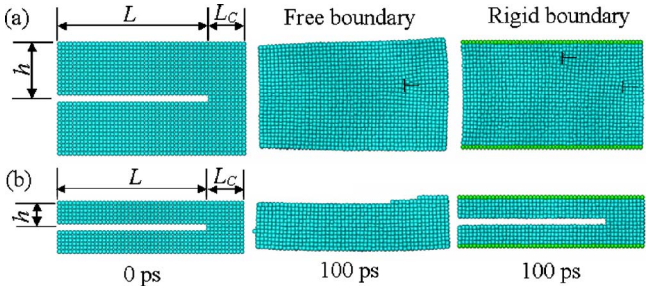


FIG. 1. (Color online) MD snapshots of a copper nanocluster with a cleavage created by removing two row atoms at 300 K under free and rigid boundary conditions for (a) $L/h=2.67$, $L/L_C=4$ and (b) $L/h=5.71$, $L/L_C=4$. The cross sections in the height directions include 30 and 14 rows of copper atoms for (a) and (b), respectively. The green atoms shown in the right figures are fixed in the three directions.

Under the free boundaries, we have shown a larger flaw by removing three rows of atoms into the same nanocluster as shown in Fig. 1(a). After a relaxation of 100 ps at 300 K, no flaw self-healing process is observed. But for the smaller nanocluster shown in Fig. 1(b), the same flaw is healed after 100 ps, as shown in Fig. 2. It is then interesting to note that the copper nanocluster has a higher flaw self-healing capability under the free boundaries when its size decreases to a compatible magnitude to the flaw length.

The effect of the temperature is studied by the MD simulations as well. For the 3100-atom Cu nanocluster under rigid boundary conditions, no self-healing is observed for the cleavagelike flaw at 300 K. However, when the system is heated to 800 K, the self-healing occurs and the defected structure is repaired. This means that increasing the temperature to a proper magnitude can improve the flaw self-healing capability under both free and rigid boundary conditions.

To investigate the effects of boundary conditions on the healing mechanism, we have calculated the potential energy of each atom for the healed nanoclusters, and the corresponding total energy distributions are plotted in Fig. 3. Under the free boundaries, the healed 7100-atom nanocluster is deformed to fill the vacancy of the removed atoms and there is a dislocation formed at the end of the flaw, which causes a high-energy region (red color) inside the cluster. However, applying the rigid boundaries, two obvious high-energy regions are found within the healed 7100-atom nanocluster, as shown in Fig. 3(b). This is because the rigid boundaries restrict the movement of the copper atoms and produce more dislocations and stress concentration regions. For the smaller 3100-atom nanocluster, the whole structure is fully released, as shown in Fig. 3(c), and no high-energy region or stress concentration appears.

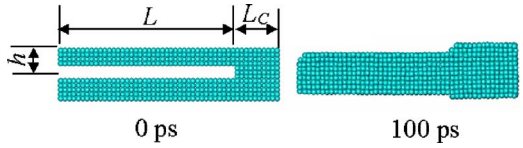


FIG. 2. (Color online) MD snapshots of 2400 atom copper nanocluster with a cleavage created by removing three row atoms at 300 K under a free boundary condition, $L/h=2.67$ and $L/L_C=4$.

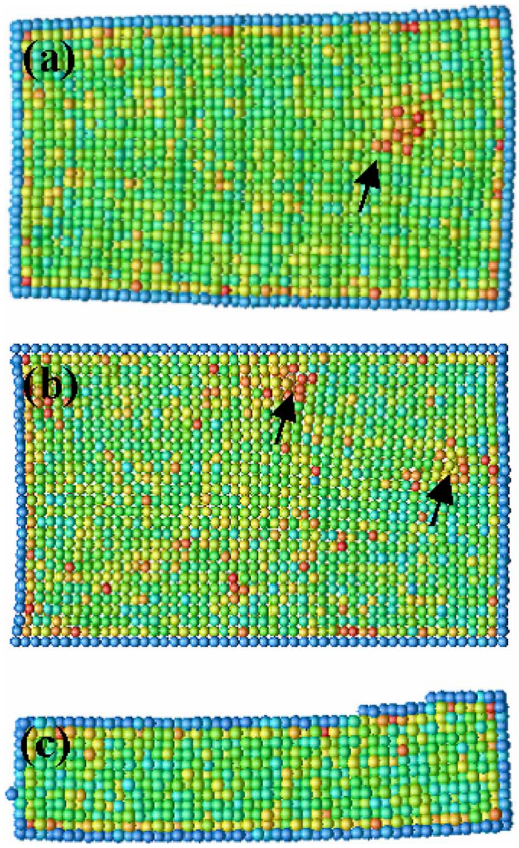


FIG. 3. (Color online) Total potential energy distribution of (a) the 7100-atom cluster under free boundary conditions, (b) the 7100-atom cluster under rigid boundary conditions, and (c) the 3100-atom cluster under free boundary conditions after 100 ps relaxations at 300 K. Blue, red, yellow, green, and cyan colors indicate the potential energy from higher to lower. Boundary atoms possess the highest potential energy, which is emphasized by the blue color. The arrows denote the dislocations.

Associating with past researches, the flaw self-healing is actually a competition process of elastic energy and surface energy, and this can be described by the continuum mechanics. Theory analysis, therefore, should be a good tool to explain and guide the molecular dynamics simulations. In the following section, we develop the procedure presented by Yu and Suo[27] to solve the flaws self-healing for different boundary conditions and compare it with our molecular dynamics simulations.

## III. THEORETICAL CONTINUUM MECHANICAL MODEL

According to Yu and Suo's theoretical model,[27] we assume that a material is divided into two individual parts along the flaw region: part one has Young's modulus $E_1$, Possion's ratio $\upsilon_1$, and thickness $t_1$ and part two with the corresponding values of $E_2$, $\upsilon_2$, and $t_2$. Figure 4 sketches a cross section of the flaw location, where the flaw has two surfaces belonging to the relevant parts, respectively. The solid curves represent the surfaces before bonding with the sinusoidal gap of flaw length $L$ and amplitude $2H$ in the $x$ direction. In the $y$ direction, the flaw has the same sinusoidal

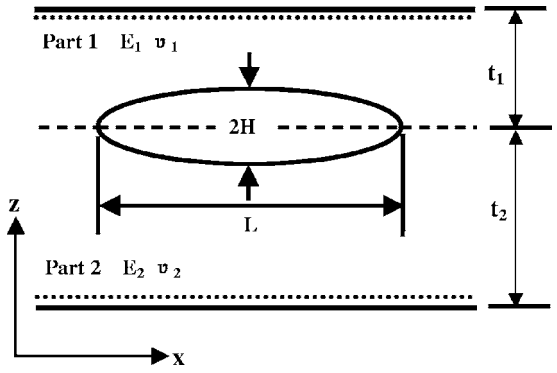


FIG. 4. The geometry of a cross section of a flaw, the material is divided into two parts along the flaw.

shape and amplitude. The dashed curve represents the assuming interface between the two parts. The attractive interatomic force between the two surfaces can lead to the full bonding and adhesion of the flaw, which effect of force can be represented by surface energies. Let $\gamma_1$ and $\gamma_2$ be the surface energies of the two parts of flaw before bonding, and $\gamma_{12}$ be the interface energy after bonding. According to the Dupre work of adhesion[27]

$$\Gamma = \gamma_1 + \gamma_2 - \gamma_{12}, \tag{1}$$

the necessary condition for the two surfaces of the flaw to adhere and heal is $\Gamma > 0$.

The ratio $H/L$ is taken to be so small that the linear elasticity theory applies. Let $(u,v,w)$ be the displacement component in the $(x,y,z)$ directions, respectively, which obey the Navier equation

$$(1-2v)u_{i,ij} + u_{j,ji} = 0. \tag{2}$$

The stresses, $\sigma_{ij}$, relate to the displacements as

$$\sigma_{ij} = \frac{E}{1+v}\left[\frac{1}{2}(u_{i,j} + u_{j,i}) + \frac{v}{1-2v}u_{k,k}\delta_{ij}\right]. \tag{3}$$

To accommodate the sinusoidal gap, the displacement field is expected to take the form[27]

$$u = \sin(kx)\cos(ky)f(kz),$$

$$v = \cos(kx)\sin(ky)f(kz),$$

$$w = w_0 + \cos(kx)\cos(ky)g(kz), \tag{4}$$

where $k=2\pi/L$, and $w_0$ represents a rigid-body translation. The coordinates $x$, $y$ are in the range of $0 \leqslant x, y \leqslant L$. The functions $f$ and $g$ are determined by substituting Eq. (4) with Eq. (2), giving

$$(1-2v)f'' - 4(1-v)f - g' = 0,$$

$$(1-v)g'' - (1-2v)g - f' = 0. \tag{5}$$

These are ordinary differential equations of constant coefficients, to which the solution is

$$f(kz) = [a_1 + a_2 kz]e^{\sqrt{2}kz} + [a_3 + a_4 kz]e^{-\sqrt{2}kz},$$

$$g(kz) = [-\sqrt{2}a_1 + (3-4v-\sqrt{2}kz)a_2]e^{\sqrt{2}kz} + [\sqrt{2}a_3 + (3-4v+\sqrt{2}kz)a_4]e^{-\sqrt{2}kz}. \tag{6}$$

The coefficients $a_i$ are to be determined by boundary conditions.

We apply the solution (6) to part one under two different boundary conditions (BC); the first is free boundary condition (BC1),[27] which includes four items: (i) on the free surface ($z=t_1$) the normal stress vanishes, namely $\sigma_{zz}=0$, (ii) on the free surface ($z=t_1$) the shear stress vanishes, $\sigma_{zx}=0$, (iii) after the flaw is healed and the two parts adhere into one interface, on the interface ($z=0$), the shear stress vanishes $\sigma_{zx}=0$, and (iv) on the interface ($z=0$) the vertical displacement of part one is

$$w_1 = -\frac{H_1}{2}[1 + \cos(kx)\cos(ky)]. \tag{7}$$

The constant $H_1$ is the amplitude of the normal surface displacement of part one. Here we use BC1 denoting the free boundary conditions and other boundary conditions are denoted like this as well. The second boundary condition (BC2) applied is a rigid boundary. The items (iii) and (iv) in the rigid boundary conditions are the same as that of the free boundary conditions, but the differences are in the items (i) and (ii). For the rigid boundary conditions; (i) on the free surface ($z=t_1$) there are no in-plane displacements in the $x$ and $y$ directions, considering the $x$ direction namely $u=0$; (ii) on the free surface ($z=t_1$) there is no vertical displacement in the $z$ direction, namely $w=0$.

According to these boundary conditions, the four $a_i$ coefficients for the two cases are determined, but they are not shown here because of the long expressions. Once these coefficients are given, all components of the displacements and stress fields are determined for part one. For simplicity, only the normal stress on the interface ($z=0$) is shown here.

For the free boundary conditions, the normal stress on the interface ($z=0$) in part one after healing is

$$(\sigma_{zz})_1 = \frac{\bar{E}_1 k H_1}{2\sqrt{2}} I(kt_1)\cos(kx)\cos(ky), \tag{8}$$

where

$$I(a) = \frac{e^{2\sqrt{2}a} + e^{-2\sqrt{2}a} - 2 - 8a^2}{e^{2\sqrt{2}a} - e^{-2\sqrt{2}a} + 4\sqrt{2}a}, \tag{9}$$

and

$$\bar{E}_1 = \frac{E_1}{1-v_1^2}. \tag{10}$$

For the rigid boundary conditions, the normal stress $(\sigma_{zz})_1$ on the interface $(z=0)$ has the same expression of the free boundary conditions, but the expression of $I(a)$ is changed to

$$I(a) = \frac{e^{2\sqrt{2}a} + e^{-2\sqrt{2}a} + \frac{10 - 24\upsilon_1 + 16\upsilon_1^2}{3 - 4\upsilon_1} + \frac{8}{3 - 4\upsilon_1}a^2}{e^{2\sqrt{2}a} - e^{-2\sqrt{2}a} - \frac{4\sqrt{2}}{3 - 4\upsilon_1}a}. \tag{11}$$

This means that Possion's ratio $\upsilon_1$ of part one will affect the stress distribution under the rigid boundary conditions and this effect should be a great difference from the free boundary conditions.

We can apply the same procedure to part two,[27] and the normal stress on the interface $(z=0)$ in part two after healing is

$$(\sigma_{zz})_2 = \frac{\bar{E}_2 k H_2}{2\sqrt{2}} I(kt_2)\cos(kx)\cos(ky). \tag{12}$$

After the flaw is healed, equilibrium requires that the normal stress on the interface be continuous, $(\sigma_{zz})_1 = (\sigma_{zz})_2$ and $H_1 + H_2 = 2H$. Then the normal stress on the interface can be obtained as

$$\sigma_{zz} = \frac{kH}{\sqrt{2}}\cos(kx)\cos(ky)\left(\frac{1}{\bar{E}_1 I(kt_1)} + \frac{1}{\bar{E}_2 I(kt_2)}\right)^{-1}. \tag{13}$$

The elastic energy stored in the two parts after complete bonding and healing can be computed by the work done by $\sigma_{zz}$ on the interface to close the misfit gap of the two flaw surfaces. The elastic energy of the joint is

$$U = \frac{1}{2}\int_0^L \int_0^L (w_2 - w_1)\sigma_{zz} dxdy, \tag{14}$$

where

$$w_2 - w_1 = \frac{H}{2}[1 + \cos(kx)\cos(ky)]. \tag{15}$$

Using the expression (13), and integrating this equation, we obtain

$$U = \frac{\pi H^2 L}{4\sqrt{2}}\left(\frac{1}{\bar{E}_1 I(kt_1)} + \frac{1}{\bar{E}_2 I(kt_2)}\right)^{-1}. \tag{16}$$

When two surfaces of the flaw transform into one interface, the free energy of the joint of flaw changes by $U - \Gamma L^2$; here $\Gamma L^2$ is the surface energy of the forming interface. Complete bonding and healing of the flaw occur if this free energy change is negative, namely[27]

$$U - \Gamma L^2 < 0. \tag{17}$$

Replacing $U$ with the expression (16), we find the critical condition of the height for the adhesion and healing of the flaw

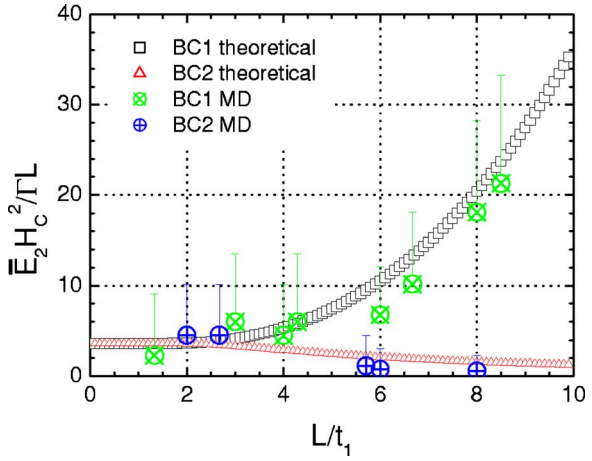


FIG. 5. (Color online) Theoretical predictions and MD simulations for the critical conditions of the flaw self-healing in Cu nanoclusters under the free and rigid boundary conditions. The error bars of MD simulations are obtained by increasing one atom layer height for the cleavagelike flaw.

$$\frac{H_C^2}{\Gamma L} = \frac{4\sqrt{2}}{\pi}\left(\frac{1}{\bar{E}_1 I(kt_1)} + \frac{1}{\bar{E}_2 I(kt_2)}\right). \tag{18}$$

Here $2H_C$ stands for the critical flaw height. If the flaw height is below the critical value, the two surfaces will bond together and the flaw is healed over the entire area. If the flaw height is beyond this critical value, the flaw cannot be healed. Free and rigid boundary conditions produce different $I(a)$ in the flaw critical height expression (18), so the boundary effects will greatly influence the flaws self-healing ability.

## IV. DISCUSSION

Using the theoretical model, we have studied the flaw self-healing capability of the Cu nanocluster under the free and rigid boundary conditions. In our calculations, the parameters $\bar{E}_2$, $\Gamma$, and $L$ are kept constant, so the dimensionless $\bar{E}_2 H_c^2/\Gamma L$ could be the critical self-healing condition. Possion's ratio $\upsilon$ of the Cu cluster is taken as 0.34 and the thickness ratio $t_2/t_1$ of the two cluster parts is 1. Figure 5 gives the variations of the critical condition $\bar{E}_2 H_c^2/\Gamma L$ with the parameter $L/t_1$ for the defected nanocluster. As the ratio $L/t_1$ is less than two, there is an evident limitation for the $\bar{E}_2 H_c^2/\Gamma L$. This means that the free and rigid boundaries produce the same critical flaw height when the nanocluster is large enough. When $L \gg t_1$, the critical height $\bar{E}_2 H_c^2/\Gamma L$ of the free boundary increases sharply with the increasing of $L/t_1$, but the critical height $\bar{E}_2 H_c^2/\Gamma L$ of the rigid boundary deceases with the increasing of $L/t_1$, and the difference in the critical conditions is remarkably enlarged.

For comparison, we also give the $\bar{E}_2 H_c^2/\Gamma L$ results of MD simulations in Fig. 5 for the same Cu nanocluster under the free and rigid boundaries. The surface energy parameter $\Gamma$ is calculated by the commonly used expression $Eb/40$, where

$E$ is Young's modulus and $b$ is the nearest atom distance. We chose the cleavagelike flaws in our MD simulations. The critical height of the healed cleavage is decided by the height of the maximum removed atom layers, and it is discrete, not continuous, in the MD simulation results. One atom layer change in the cleavage height will lead to a great difference in the final result of $\bar{E}_2 H_c^2/\Gamma L$. Therefore, Fig. 5 gives the possible error of the critical self-healing condition by increasing one atom layer height for the flaw. Comparing the MD simulation with theoretical analysis, most of the MD simulation results agree well with the variations of theoretical predictions. Decreasing the material size, the free boundaries improve the flaw self-healing capability but the rigid boundaries weaken this capability. Due to different flaw shape hypothesis and temperature effects in the MD simulations, there are some differences between the MD and theoretical results, but the theoretical variations still locate in the error range of MD simulations. The consistency of the MD simulation with the theoretical calculations proves nicely the strong boundary and size effects on the flaws self-healing properties in nanoscale materials.

In terms of Eq. (18), the critical condition of height $H_C$ is directly related to Young's modulus and the flaw length $L$. Lower Young's modulus lead to a higher height $H_C$, and this, accordingly, improves the flaws self-healing capability. On the other hand, keeping the ratios $L/t_1$ and $L/t_2$ unchanged by modifying $t_1$ and $t_2$ values in the expression (18), as well as increasing the flaw length $L$ can increase the critical height $H_C$ under both the free and rigid boundaries. This theoretical prediction of the flaw length effects also coincides with the MD simulation results.

## V. FLAW SELF-HEALING IN BIOMATERIALS

In multilamella structure of biomaterials as mentioned above, both the mineral and protein lamellae are in the scale of nanometer. Because of their interactions and different elastic modulus, the protein layer produces soft boundary restriction effects on the aragonite layer. These boundary effects are not completely equal to the free or rigid boundaries because the surface of the lamella may be stretched or compressed due to the interlayer interactions. To investigate the boundary effects on the flaws self-healing properties in biomaterials, we use the same theoretical procedure but two different force boundary conditions are introduced on the mineral layer surfaces. The first force boundary conditions (BC3) are: (i) on the free surface ($z=t_1$), we assume the normal stress increases linearly with the surface vertical displacement, namely $\sigma_{zz}=\bar{K}_1 w$, where $\bar{K}_1$ is an appropriate elastic modulus; (ii) on the surface ($z=t_1$) there are no in-plane displacements in the $x$ and $y$ directions, only considering the $x$ direction, namely $u=0$, the items (iii) and (iv) are the same as that of the free boundary conditions (BC1). The second force boundary conditions (BC4) are almost the same as that of the first force boundary conditions, the only difference is item (ii): on the surface ($z=t_1$) the shear stress vanishes, namely $\sigma_{zx}=0$. The hard or soft boundary effects existing on the surfaces of the mineral layer are realized by adjusting the appropriate force constant $\bar{K}_1$. Solving these two kinds of force boundary conditions, the obtained normal stress $\sigma_{zz}$ expressions on the interface as well as the final critical height expressions are the same as the previous results of other boundary conditions, but the $I(a)$ is changed. For the case of the first force boundary conditions (BC3), we let $I(a)$ equal to

$$I(a) = I_1(a)/I_2(a), \tag{19}$$

where

$$I_1(a) = e^{2\sqrt{2}a} + \frac{(1-v_1)+K}{-(1-v_1)+K} e^{-2\sqrt{2}a} + \frac{2K(5-12v_1+8v_1^2)/(3-4v_1) + 4\sqrt{2}(1-v_1)a + 2\sqrt{2}(1+v_1)a^2}{-(1-v_1)+K}, \tag{20}$$

$$I_2(a) = e^{2\sqrt{2}a} - \frac{(1-v_1)+K}{-(1-v_1)+K} e^{-2\sqrt{2}a} - \frac{2(1-v_1)+4\sqrt{2}K/(3-4v_1)}{-(1-v_1)+K} a, \tag{21}$$

$$K = \frac{\sqrt{2}}{4} \frac{\bar{K}_1}{E_1 k} (1+v_1)(3-4v_1). \tag{22}$$

For the second force boundary conditions (BC4), we also let $I(a)$ equal to

$$I(a) = I_1(a)/I_2(a),$$

but $I_1(a)$ and $I_2(a)$ are changed

$$\begin{aligned} I_1(a) = {} & \left(-1 + e^{4\sqrt{2}a} + 4\sqrt{2}a e^{2\sqrt{2}a}\right)\left[-1 - e^{4\sqrt{2}a} + 2(1 + 4a^2)e^{2\sqrt{2}a}\right] - 2\left(1 - e^{2\sqrt{2}a}\right)^2 K^2 \left(-1 + e^{4\sqrt{2}a} + 4\sqrt{2}a e^{2\sqrt{2}a}\right) - 2K\left[-\sqrt{2} - \sqrt{2}e^{8\sqrt{2}a} - 2\sqrt{2}(1 + 12a^2)e^{4\sqrt{2}a}\right] + 4K\left[\left(\sqrt{2} - 4a + 2\sqrt{2}a^2\right)e^{6\sqrt{2}a} + \left(\sqrt{2} + 4a + 2\sqrt{2}a^2\right)e^{2\sqrt{2}a}\right], \end{aligned} \tag{23}$$

$$I_2(a) = -\left[\left(-1 + e^{4\sqrt{2}a} + 4\sqrt{2}a e^{2\sqrt{2}a}\right) - \sqrt{2}K\left(1 - e^{2\sqrt{2}a}\right)^2\right]^2, \tag{24}$$

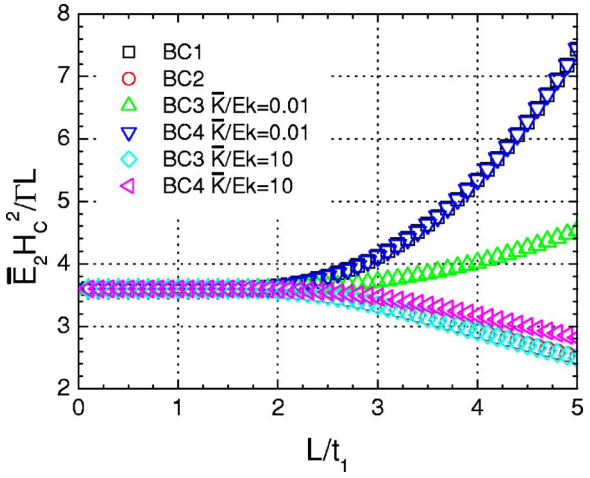


FIG. 6. (Color online) The critical conditions for the flaw healing inside the mineral layer under different boundary conditions, $\bar{E}_1/\bar{E}_2=1$, $t_2/t_1=1$, $\bar{K}/Ek=0.01$, and $\bar{K}/Ek=10$.

$$K=(1-v_1^2)\frac{\bar{K}_1}{E_1 k}. \tag{25}$$

Checking these results, the critical height $H_C$ is determined not only by the Possion ratio and Young's modulus but also by the appropriate force constant $\bar{K}_1$. Details of the theoretical analysis for the flaws self-healing in biomaterial are presented in the following part.

Figure 6 displays the critical conditions of flaw self-healing inside mineral layers under different boundary conditions. The parameters $\bar{E}_1/\bar{E}_2=1$ and $t_2/t_1=1$ means that the flaw just locates in the middle of the aragonite layer. For simplicity, we assume all the materials possessing the same Possion's ratio of 0.3. The external loading as well as the force boundary effects are denoted by the parameter $\bar{K}/Ek$. Here we assume $\bar{K}/Ek=0.01$, representing a soft boundary with the mineral layer contacting with a protein layer, and $\bar{K}/Ek=10$, representing a hard boundary with the mineral layer directly contacting with other mineral layer. Everything is equal and no boundary effects occur when the ratio of the flaw length and material thickness $L/t_1<2$. After that, for the case of $\bar{K}/Ek=0.01$, the critical conditions $\bar{E}_2H_c^2/\Gamma L$ of BC3 and BC4 are increasing with the increasing of $L/t_1$. However, when the corresponding force parameter $\bar{K}/Ek$ increases to 10 and the boundary is harder, the flaws self-healing capability decreases with the $L/t_1$ increasing, and the two variations of BC3 and BC4 almost overlap with that of the rigid boundary conditions (BC2). For the same $L/t_1$, the critical height of $H_c$ under soft boundary conditions is obviously higher than that of the hard boundary conditions. That means the mineral layer possesses a higher flaw self-healing capability when it contacts with a protein layer. As the parameter $\bar{K}/Ek$ approaches 0 and infinity, the variations are evolved to their limited cases of the free and rigid boundaries, respectively.

Except inside the interior of the lamella, the flaws self-healing problem in the interface between the aragonite and protein layers can be solved using this procedure as well. We use part one and part two to represent the protein layer and the aragonite layer, respectively. According to the experimental observations, we chose the thickness ratio $t_2/t_1$ of the aragonite and protein layers to be 40. The mineral layer is much stiffer than the protein layer, so we assume their Young's modulus ratio $\bar{E}_1/\bar{E}_2=0.1$ and 0.01. The variations of $\bar{E}_2H_c^2/\Gamma L$ for these cases are plotted in Fig. 7. Comparing these curves, it is interesting to find that the critical condition $\bar{E}_2H_c^2/\Gamma L$ of $\bar{E}_1/\bar{E}_2=0.01$ is about 10 times higher than that of $\bar{E}_1/\bar{E}_2=0.1$ at each corresponding abscissa $L/t_1$. Softer protein possesses better deformability and flowing behaviors so that it could easily repair the possible defects on the surface of the mineral layer, and hence improve the flaws self-healing capability in biomaterials.

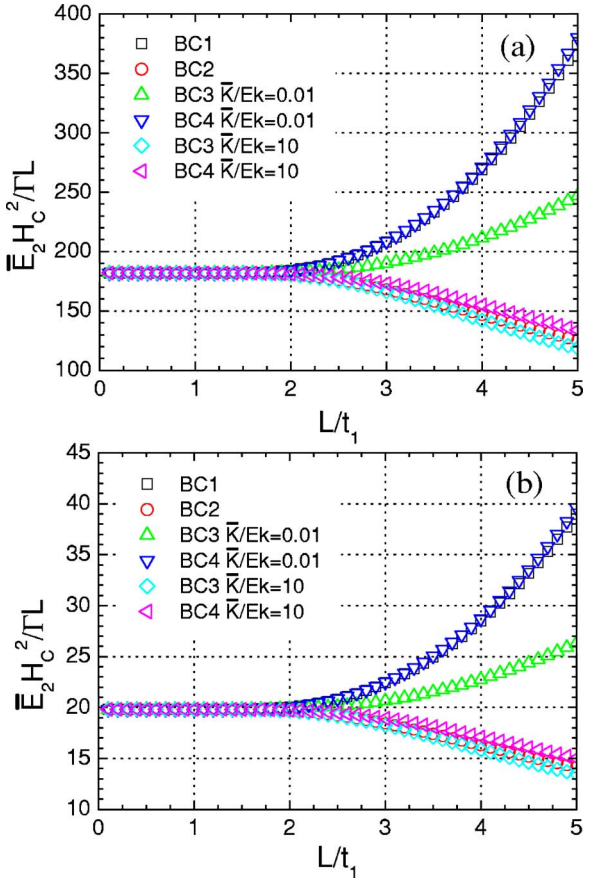


FIG. 7. (Color online) The critical conditions for the flaw healing inside the interface of mineral and protein layers under different boundary conditions. (a) $\bar{E}_1/\bar{E}_2=0.01$, $t_2/t_1=40$ and (b) $\bar{E}_1/\bar{E}_2=0.1$, $t_2/t_1=40$.

## VI. SUMMARY

The flaw or crack self-healing capabilities in a nanoscale material are very sensitive to its boundary conditions when the material size decreases to a compatible magnitude to its defect. For a Cu nanocluster, the free boundaries improve the flaw or crack self-healing capability, but the rigid boundaries

weaken this capability remarkably. We develop the continuum mechanical theory model by presenting various boundary conditions, and the theoretical predictions agree well with the molecular dynamics simulations. Soft boundaries, increasing temperature in a suitable range, decreasing the cluster size as well as a lower Young's modulus can improve the flaw or crack self-healing capabilities. Further theoretical investigations show that the mineral layer in biomaterials has a high flaw self-healing capability because of the natural soft boundaries caused by the protein layer. Our study provides an explanation for the self-optimization process in biomaterial evolution.

## ACKNOWLEDGMENTS

This work was supported by the national and Jiangsu Province NSFs.

*Corresponding author. Email address: wlguo@nuaaa.edu.cn

[1] M. S. Gudiksen, L. J. Lauhon, J. F. Wang, D. C. Smith, and C. M. Lieber, Nature (London) **415**, 617 (2002).
[2] S. Iijima, Nature (London) **354**, 56 (1991).
[3] M. R. Buitelaar, A. Bachtold, T. Nussbaumer, M. Iqbal, and C. Schönenberger, Phys. Rev. Lett. **88**, 156801 (2002).
[4] A. V. Ellis, K. Vijayamohanan, R. Goswami, N. Chakrapani, L. S. Ramanathan, P. M. Ajayan, and G. Ramanath, Nano Lett. **3**, 279 (2003).
[5] W. L. Guo and Y. F. Guo, Phys. Rev. Lett. **91**, 115501 (2003).
[6] Y. F. Guo and W. L. Guo, J. Phys. D **36**, 805 (2003).
[7] Y. F. Guo, Y. Kong, H. J. Gao, and W. L. Guo, J. Comput. Theor. Nanosci. **1**, 93 (2004).
[8] D. F. Urban, J. Bürki, C. H. Zhang, C. A. Stafford, and H. Grabert, Phys. Rev. Lett. **93**, 186403 (2004).
[9] Z. W. Liu, Y. Bando, M. Mitome, and J. Zhan, Phys. Rev. Lett. **93**, 095504 (2004).
[10] Q. Sun, Q. Wang, B. K. Rao, and P. Jena, Phys. Rev. Lett. **93**, 186803 (2004).
[11] M. Rubner, Nature (London) **423**, 925 (2003).
[12] H. J. Gao, B. H. Ji, I. L. Jager, E. Arzt, and P. Fratzl, Proc. Natl. Acad. Sci. U.S.A. **100**, 5597 (2003).
[13] R. Z. Wang, Z. Suo, A. G. Evans, N. Yao, and I. A. Aksay, J. Mater. Res. **16**, 2485 (2001).
[14] H. Kessler, R. Ballarini, R. L. Mullen, L. T. Kuhn, and A. H. Heuer, Comput. Mater. Sci. **5**, 157 (1996).
[15] K. Okumura and P. G. de Gennes, Eur. Phys. J. E **4**, 121 (2001).
[16] S. Weiner and L. Addadi, J. Mater. Chem. **7**, 689 (1997).
[17] S. Weiner, A. Veis, E. Beniash, T. Arad, J. W. Dillon, B. Sabsay, and F. Siddiqui, J. Struct. Biol. **126**, 27 (1999).
[18] J. Y. Rho, L. Kuhn-Spearing, and P. Zioupos, Med. Eng. Phys. **20**, 92 (1998).
[19] S. Weiner and H. D. Wagner, Annu. Rev. Mater. Sci. **28**, 271 (1998).
[20] R. Menig, M. H. Meyers, M. A. Meyers, and K. S. Vecchio, Mater. Sci. Eng., A **297**, 203 (2001).
[21] S. Kamat, X. Su, R. Ballarini, and A. H. Heuer, Nature (London) **405**, 1036 (2000).
[22] X. D. Li, W. C. Chang, Y. J. Chao, R. Z. Wang, and M. Chang, Nano Lett. **4**, 613 (2004).
[23] A. P. Jackson, J. F. V. Vincent, and R. M. Turner, Proc. R. Soc. London, Ser. B **234**, 415 (1988).
[24] W. Tesch, N. Eidelman, P. Roschger, F. Goldenberg, K. Klaushofer, and P. Fratzl, Calcif. Tissue Int. **69**, 147 (2001).
[25] W. J. Landis, Bone (N.Y.) **16**, 533 (1995).
[26] W. J. Landis and K. J. Hodgens, J. Struct. Biol. **117**, 24 (1996).
[27] H. H. Yu and Z. Suo, J. Mech. Phys. Solids **46**, 829 (1998).
[28] S. Li, K. W. Gao, L. J. Qiao, F. X. Zhou, and W. Y. Chu, Comput. Mater. Sci. **20**, 143 (2001).
[29] M. S. Daw and M. I. Baskes, Phys. Rev. B **29**, 6443 (1984).